Turkish Journal of Physics

http://journals.tubitak.gov.tr/physics/

Research Article

Turk J Phys
(2018) 42: 675 – 687

doi:10.3906/fiz-1807-6

Triple Higgs boson production in a $\gamma\gamma$-collider at the future linear collider

Nasuf SÖNMEZ*
Department of Physics, Faculty of Science, Ege University, İzmir, Turkey

Received: 04.07.2018 • **Accepted/Published Online:** 02.11.2018 • **Final Version:** 14.12.2018

Abstract: In this study, triple Higgs boson production channels in a $\gamma\gamma$-collider are investigated in the context of the two-Higgs-doublet model (2HDM). This model has three neutral Higgs bosons ($h^0/H^0/A^0$) and two charged Higgs bosons ($H^\pm$). Between all the possible combinations of the triple Higgs bosons in the final state, only the following two scattering processes are probable at tree-level: $\gamma\gamma \to H^+H^-h^0$ and $\gamma\gamma \to H^+H^-H^0$. These two processes are important to determine the triple Higgs self-couplings $g_{H^+H^-h^0}$ and $g_{H^+H^-H^0}$ in the 2HDM. The calculation is carried out for two scenarios, which are inspired by recent experimental and theoretical results. The cross-section of these processes is calculated and a comparison is made for these scenarios. The total convoluted cross-section with photon luminosity in an e^+e^--collider is presented as a function of the center of mass energy.

Key words: Two-Higgs-doublet model, 2HDM, photon–photon collider, triple Higgs production, triple Higgs self-couplings

1. Introduction

The discovery of the Higgs boson at CERN [1–3] is an undeniable solid experimental proof of the electroweak symmetry breaking mechanism that makes it possible to give mass to the Goldstone bosons. It was the last missing piece of the standard model (SM). However, there are still loose ends in the SM, and the answers are sought in the new models that extend the SM. There are many proposals, and many of them predict new symmetries, interactions, and particles. One of them is obtained by extending the scalar sector of the SM, and it is called the two-Higgs-doublet model (2HDM). The new doublet has the same quantum number by definition so that it couples to quarks and leptons. The model predicts five scalar particles and new vertices for them. Some of the predictions were already tested in the previous colliders and negative results were obtained. Although the LHC is powerful enough to test these theories and their predictions, no conclusive result has been obtained so far. Besides the LHC, there are continuing studies for possible future colliders. In these colliders, e^+e^-, γe, and even $\gamma\gamma$ collisions have been proposed. Recently, the efforts put into the ILC [4] and the CLIC [5] projects were combined towards the next collider, which is called the Linear Collider Collaboration (LCC) [6]. It is assumed that the future lepton colliders will have a cleaner background, and the new physics signals could be extracted more easily from the background. The primary task of the LCC will be to complement and improve the results obtained at the LHC, and also to hunt for clues beyond the SM. The detectors sitting on the LCC beam-line are designed to study the properties of new hypothetical particles and the interactions they have. The $\gamma\gamma$-collider is considered as a future option with an integrated luminosity of the order of 100 fb^{-1}

*Correspondence: nasuf.sonmez@ege.edu.tr

yearly [4]. The machine is expected to be upgradeable to $\sqrt{s} = 1$ TeV with a total integrated luminosity up to 300 fb^{-1} yearly.

The production of triple Higgs bosons was investigated before to determine the Higgs self-couplings. In the SM, there is only one triple Higgs self-coupling, g_{HHH}, but in the 2HDM there is a total of eight triple Higgs self-couplings [7]. Investigating these couplings in lepton colliders is a hot research topic studied extensively. This paper explores the potential of a $\gamma\gamma$-collider regarding the triple Higgs production in the 2HDM. In general, there are various possible triple Higgs final states in the 2HDM, but in a $\gamma\gamma$-collider only the following final states are accessible at tree-level while the CP is conserved: $H^+H^-h^0$ and $H^+H^-H^0$. These two processes and the Higgs sector regarding the $\gamma\gamma$-collider will be investigated here. The triple Higgs production was studied before in the context of the MSSM in e^+e^--colliders. However, the relevant triple Higgs self-couplings in the 2HDM could be large compared to the MSSM because the supersymmetry suppresses the quartic couplings by associating them with the gauge couplings [8]. The charged Higgs pair production in e^+e^--colliders was investigated extensively in the MSSM [9–11] and the 2HDM [12, 13]. The scattering processes $e^+e^- \to H^+H^-h^0/H^0$ were also investigated previously [14, 15, 17] with different motivations. A similar study with the same processes was presented for the Higgs triplet model [18]. In the present work, the triple Higgs boson production in the 2HDM is studied, and particularly the two processes $\gamma\gamma \to H^+H^-h^0$ and $\gamma\gamma \to H^+H^-H^0$ are investigated. Some limits on the free parameters in the 2HDM are assumed by taking into account various restrictions set in the previous experiments. The numerical analysis for the triple Higgs production is presented using these limits. The cross-section values as a function of the center-of-mass (c.m.) energy and the dependence on the free parameters of the model are calculated. In addition to these, the convoluted cross-section ($e^+e^- \to \gamma\gamma \to H^+H^-(h^0/H^0)$) with photon luminosity in an e^+e^- collider is presented up to $\sqrt{s} = 3$ TeV.

The paper is organized as follows. In Section 2, the scalar sector of the 2HDM is presented briefly. The scattering processes and the machinery of the computation are given in Section 3. The theoretical and the recent experimental constraints that restrict the 2HDM, the parameter space, and the region of interest are discussed in Section 4. Next, the numerical results of the total cross-section for various scenarios are presented in Section 5. Finally, a conclusion is outlined in Section 6.

2. The scalar sector of the 2HDM

In this section, scalar potential, interactions, and free parameters in the 2HDM, which are relevant to the computation, are presented. The model is obtained by extending the SM Higgs sector by a second $SU_L(2)$ doublet with a weak hypercharge $Y = 1$. The Higgs doublets in the generic basis are defined as follows:

$$\phi_i = \begin{bmatrix} w_i^+ \\ \frac{1}{\sqrt{2}}(v_i + h_i + iz_i) \end{bmatrix}, \quad (i = 1, 2), \tag{1}$$

where the vacuum expectation values are given as $< \phi_i >_0 = \frac{1}{\sqrt{2}} \begin{pmatrix} 0 \\ v_i \end{pmatrix}$, and they satisfy $v = \sqrt{v_1^2 + v_2^2} = 246$ GeV. In general, the 2HDM has many parameters, but most phenomenological studies consider several assumptions that simplify the scalar potential in the 2HDM. In this study, we consider the 2HDM with CP-conservation, additionally introducing a discrete symmetry ($\mathcal{Z}_2$) that restricts the most general form of the Higgs scalar potential and the Higgs–fermion interactions [19–21]. The flavor-changing neutral currents are

avoided at tree-level under this discrete symmetry. Therefore, the scalar potential becomes the following:

$$\begin{aligned} V_{\rm 2HDM}(\phi_1,\phi_2) &= m_1^2|\phi_1|^2+m_2^2|\phi_2|^2-\left[m_3^2\phi_1^\dagger\phi_2+h.c.\right] \\ &+\frac{\lambda_1}{2}|(\phi_1^\dagger\phi_1)^2+\frac{\lambda_2}{2}(\phi_2^\dagger\phi_2)^2+\lambda_3|\phi_1|^2|\phi_2|^2 \\ &+\lambda_4|\phi_1^\dagger\phi_2|^2+\left[\frac{\lambda_5}{2}(\phi_1^\dagger\phi_2)^2+h.c.\right]. \end{aligned} \tag{2}$$

In general, the parameters λ_{1-4}, m_1, and m_2 are taken as real while λ_5 and m_3 could be complex. However, m_3 and λ_5 are taken as real because CP-violation is not taken into account at tree-level in this study.

The new scalar states along with their masses and the interaction vertices between them are obtained from the scalar potential given in Eq. (2). The prescription was already given before in the literature [22, 23]; therefore, they will be mentioned only briefly here. The ground state conditions are obtained with the aid of $\partial V/\partial\phi_i = 0$, for i=1,2, and these relate m_1^2 and m_2^2 to the other parameters in the scalar potential. Then substituting them into the scalar potential eliminates these mass parameters. It is argued that it is convenient to study the model in the so-called *Higgs basis* [22]. In this basis, the Higgs doublets are rotated by angle $\sin\beta = v_2/v$ and $\cos\beta = v_1/v$. The new doublets are defined as follows: $H_1 = \phi_1\cos\beta+\phi_2\sin\beta$ and $H_2 = -\phi_1\sin\beta+\phi_2\cos\beta$. If the Higgs doublets are substituted into Eq. (2), then the Higgs potential $V_{\rm 2HDM}$ decomposes into several terms, namely a quadratic term, which give the masses of Higgs bosons ($h^0/H^0/A^0/H^\pm$), plus cubic and quartic terms, which define the interactions in the model. According to the electroweak symmetry breaking, 3 degrees of freedom are eaten by the Goldstone bosons, and the electroweak messenger particles acquire mass. The remaining degrees of freedom form the prominent property of the model: two charged and three neutral Higgs bosons [7]. The Higgs basis serves to diagonalize the mass matrices of w_i^+ fields and z_i fields defined in Eq. (1) so that the charged scalar states $H^\pm$ and CP-odd scalar state A^0 are obtained, respectively. Then another parameter is introduced that helps to diagonalize the mass matrix of the neutral states (h_i) and that defines the CP-even states (h^0/H^0). That parameter is called α, and along with the previous rotation β, the total rotation matrix becomes a function of $s_{\beta-\alpha} = \sin(\beta-\alpha)$ and $c_{\beta-\alpha} = \cos(\beta-\alpha)$. More detailed discussion is available in the literature [22, 23].

Under these assumptions and substitutions, the parameters in the Higgs potential could be related to the masses of the Higgs states. Thus, instead of working with the parameters in Eq. (2), the model could be analyzed as a function of the following parameters: the masses of the neutral Higgs bosons ($m_{h/H^0/A^0}$) and the charged Higgs bosons ($m_{H^\pm}$), the vacuum expectation value ($v = 246$ GeV), the ratio of the vacuum expectation values ($\tan\beta = v_2/v_1$), the mixing angle ($s_{\beta-\alpha}$) between the CP-even neutral Higgs states, and the soft breaking scale of the discrete symmetry (m_3^2). Working with so many parameters makes it hard to study the model. They could be constrained by experimental results and theoretical assumptions, which are discussed in Section 3.

3. The Calculation of the cross-section

In this section, the machinery of the computation is expressed and some of the relations linked with the cross-section in the $\gamma\gamma$-collider and e^+e^--collider (the convolution over the photon luminosity) are underlined briefly.

The scattering processes are denoted as follows:

$$\gamma(k_1) + \gamma(k_2) \;\rightarrow\; H^+(k_3) + H^-(k_4) + h^0/H^0(k_5),$$

where k_a $(a = 1, ..., 5)$ are the four momenta of the incoming photons and outgoing Higgs bosons.

In a $\gamma\gamma$ collision, two processes are possible at tree-level with the assumptions made in the previous section, and they are $\gamma\gamma \to H^+H^-h^0$ and $\gamma\gamma \to H^+H^-H^0$. The relevant Feynman diagrams that take part in the processes given above are depicted in Figure 1. These diagrams and amplitudes are generated using FeynArts [24] and the couplings defined in the build-in model file named `THDM.mod`. Next, the amplitudes are simplified, and the total amplitude is squared for further numerical calculation with the help of FormCalc [25]. The couplings involved in each of the scattering processes that are investigated in this paper are $g_{\gamma\gamma H^+H^-}$, $g_{\gamma H^+H^-}$, and $g_{H^+H^-[h^0,H^0]}$ [14, 15]. They are given in Table 1. The first two couplings are in a sense universal, and they are obtained from the kinetic energy term of the Higgs fields. However, the other couplings, $g_{H^+H^-h^0}$ and $g_{H^+H^-H^0}$, are functions of the free parameters of the 2HDM, and they are obtained from V_{2HDM}. The Higgs self-couplings agree with reference [16]. The couplings involved in the scattering process $\gamma\gamma \to H^+H^-h^0$ are $g_{\gamma\gamma H^+H^-}$, $g_{\gamma H^+H^-}$, and $g_{H^+H^-h^0}$. The same couplings are involved in the process $\gamma\gamma \to H^+H^-H^0$ with one difference: the coupling $g_{H^+H^-h^0}$ is exchanged with the $g_{H^+H^-H^0}$.

Table 1. The relevant couplings involved in each of the scattering processes. c and s represent cosine and sine functions, respectively. The subindex is the relevant mixing angle α or β, whereas $\alpha\beta = (\alpha + \beta)$ and $\beta\alpha = (\beta - \alpha)$ represent the combination of them.

$g_{H^+H^-\gamma\gamma}$	$2ie^2$
$g_{H^+H^-\gamma}$	ie
$g_{H^+H^-h^0}$	$\frac{i}{v}\left((m^2_{h^0} - 2m^2_{H^\pm})s_{\beta\alpha} - (2m^2_{h^0} - \frac{2m_3^2}{s_\beta c_\beta})\frac{c_{\alpha\beta}}{2s_\beta c_\beta}\right)$
$g_{H^+H^-H^0}$	$\frac{i}{v}\left((m^2_{H^0} - 2m^2_{H^\pm})c_{\beta\alpha} - (2m^2_{H^0} - \frac{2m_3^2}{s_\beta c_\beta})\frac{s_{\alpha\beta}}{2s_\beta c_\beta}\right)$

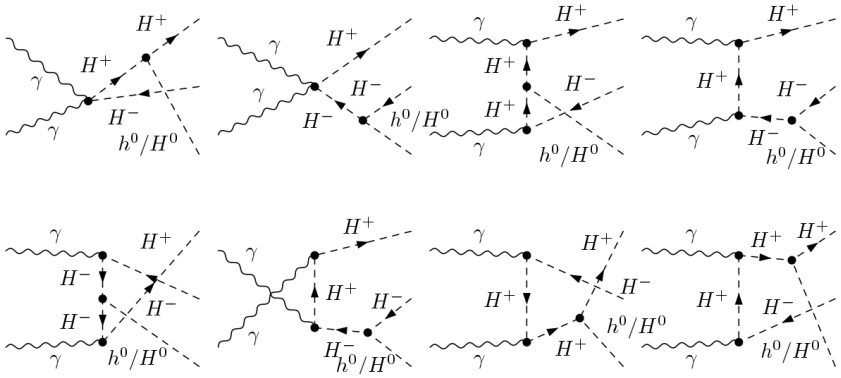

Figure 1. Feynman diagrams at tree-level for the production of the charged Higgs pair associated with the CP-even neutral Higgs bosons via $\gamma\gamma$ collision.

The corresponding Lorentz invariant matrix element $\mathcal{M}_{tot}^{\text{process}}$ is written as a sum over the diagrams presented in Figure 1, and the cross-section is calculated in the c.m. frame. The differential cross-section is

defined as follows:

$$\frac{d\sigma_{\gamma\gamma\to\text{Triple Higgs}}(\hat{s})}{dk_5^0 dk_3^0 d\cos\theta\, d\eta} = \frac{1}{16\,\hat{s}\,(2\pi)^4}\left(\frac{1}{4}\sum_{pol}|\mathcal{M}_{tot}^{\text{process}}|^2\right), \tag{3}$$

where the average over the polarization of the photons is taken. The Monte-Carlo integration methods are employed over the phase space of the final states.

In the future linear electron-positron colliders, it is possible to produce high energetic γ-rays, such that a linear e^+e^--collider could be transformed to produce $\gamma\gamma$ collisions. In that case, the cross-section in Eq. (3) needs to be convoluted over the photon luminosity. The convoluted cross-section is defined as follows:

$$\sigma(s) = \int_{y_{min}}^{y_{max}} \frac{dL_{\gamma\gamma}}{dz}\hat{\sigma}_{\gamma\gamma\to\text{Triple Higgs}}(\hat{s};\ \hat{s}=z^2 s)\, dz\,, \tag{4}$$

where s and $\hat{s}$ represent the c.m. energy in a linear e^+e^--collider and $\gamma\gamma$ collisions, respectively. $y_{min} = (m_{H^+} + m_{H^-} + m_{h^0/H^0})/\sqrt{s}$ is the threshold energy for producing the particles in the final state. A detailed discussion is delivered in references [26, 27]. The maximum energy fraction of the backscattered photons is defined as $y_{\max} = x/(1+x)$, where $x = \left(4E_0 w_0/m_e^2\right)\cos(\alpha_0^2/4)$. $y_{\max}$ increases with the energy of the incoming electron beam because photons with energy E_0 are scattered by a laser with $w_0 = 1.17$ eV from the electrons at a small collision angle $\alpha_0 = 2\cdot 10^{-6}$. The energy spectrum of the photons is defined in Eqs. (3) and (4) in reference [26],and the mean helicity λ_e (polarization P_c) of the initial electron beams (laser photon) is assumed as $\lambda_e \cdot P_c = -1$ because the number of high energetic photons is increased. The photon luminosity is defined in the formula given below:

$$\frac{dL_{\gamma\gamma}}{dz} = 2z\int_{z^2/y_{max}}^{y_{max}} \frac{dx}{y} F_{\gamma/e}(y) F_{\gamma/e}\left(\frac{z^2}{y}\right), \tag{5}$$

where $F_{\gamma/e}(y)$ is the energy spectrum of the Compton backscattered photons from the initial electrons [26]. However, it should be noted that extending the photon spectrum to higher energies ($\sqrt{\hat{s}} > 500$ GeV) is an approximation because the real luminosity spectrum is unknown [28]. Besides, the convolution is carried out by considering that the interaction point and the convergence point are overlapped ($\rho = 0$) [29]. These approximations are considered to assess the potential of the $\gamma\gamma$-collider regarding triple Higgs production.

4. Constraining the parameter space of the 2HDM and benchmark points

The constraints that are applied to the free parameters of the 2HDM could be divided into two sets: theoretical and experimental. In this section, these constraints are reviewed, and the region of interest of the parameter space is discussed.

4.1. Theoretical constraints

- *Vacuum stability*: The scalar potential (V_{2HDM}) needs to be bounded from below. In other words, it needs to be positive in any direction of the field space even at asymptotically large values [20, 30–32]. This constraint translates into the following conditions, and note that the third one applies if $\lambda_6 = \lambda_7 = 0$ [30]:

$$\lambda_1 > 0, \quad \lambda_2 > 0,$$
$$\lambda_3 + \sqrt{\lambda_1 \lambda_2} > 0,$$
$$\sqrt{\lambda_1 \lambda_2} + \lambda_3 + min(0, \lambda_4 - |\lambda_5|) > 0.$$

- *Perturbative unitarity*: The scattering cross-section of the longitudinal W-bosons tends to rise with increasing energy. When the Higgs exchange diagram is included as in the SM, that rise falls, and the theory becomes unitary. The basic idea is that the scattering amplitudes need to be flat at asymptotically large energies. In the 2HDM, the same argument applies; however, due to the additional Higgs states in the model, we need to ensure that all the scattering amplitudes of Higgs-Higgs and Higgs-vector bosons (longitudinal mode) are bounded by 16π [33].

- *Perturbativity*: The theory must be inside the perturbative region. If the Higgs quartic self-couplings get large, the scalar sector becomes strongly coupled. Therefore, all the quartic Higgs self-couplings need to be small from a particular value ($|g_{H_i H_j H_k H_l}| \leq 4\pi$).

4.2. Experimental constraints

- The 2HDM needs to be compatible with all the electroweak observables that were measured in the previous experiments [34]. There are parameters that are called the oblique parameters (S, T, and U) [35, 36], and they represent the radiative corrections to the two-point correlation functions of the electroweak gauge bosons. These parameters are sensitive to any new physics contributions, and they are set to vanish for a reference point in the SM so $S = T = U = 0$. According to that, a sizable deviation from zero would be an indicator for the existence of new physics. These parameters were calculated before in references [37–40]. In this study, they are numerically checked with the help of 2HDMC [41], and all of them are less than $5 \cdot 10^{-3}$ for the whole region.

- ATLAS and CMS experiments have reported the long-sought resonance with the mass of 125.4 ± 0.4 GeV [2, 3, 42]. We know that the announced peak must have a nature of CP-even. Therefore, that peak needs to correspond to one of the CP-even h^0 or H^0 states in the 2HDM. In the computation, we examined both of the possibilities and investigated the implications on each of the processes. If we assume h^0 is the discovered resonance at the LHC, that limits the parameter $s_{\beta-\alpha}$ and pushes it to unity. The second possibility is that H^0 is the discovered one at the LHC; then $c_{\beta-\alpha}$ is set to unity. However, due to phenomenological curiosity, we let these factors ($s_{\beta-\alpha}$ and $c_{\beta-\alpha}$) deviate from unity in both cases.

- The LEP experiment excluded the charged Higgs boson with mass below 80 GeV (Type II scenario) or 72.5 GeV [43] (Type I scenario, for pseudo-scalar masses above 12 GeV) at the 95% CL. If it is assumed that $BR(H^+ \to \tau^+ \nu) = 1$, then the charged Higgs mass bound is increased to 94 GeV for all $\tan\beta$ values [43]. The Tevatron experiments D0 [44–46] and CDF [47] excluded the charged Higgs mass in the range of 80 GeV $< m_{H^\pm} <$ 155 GeV at the 95% CL. The charged Higgs was studied at the LHC in the decay of the top quark [48, 49], and upper limits were set for $BR(t \to H^+ b)$ and $BR(H^+ \to \tau\nu)$. More recent results were given in reference [50] and the references therein.

4.3. Region for the analysis

After introducing all these constraints coming from the theory and the experiments in the previous subsections, we need to define a region for the free parameters defined in Section 2. In this study, inspired by reference [23], the following two scenarios are considered.

- ***Scenario A***: In this scenario, the particle with mass of 125 GeV is assumed as the CP-even Higgs boson (h^0) with SM-like couplings. In this limit, $|c_{\beta-\alpha}| \to 0$, and the coupling c_{h^0VV} approaches the SM value. Therefore, the heavier brother CP-even Higgs boson (H^0) can not decay into a vector boson pair. The results coming from the flavor physics favor the exact alignment limit $s_{\beta-\alpha} = 1$ and $c_{\beta-\alpha} = 0$. However, to allow some interesting phenomenology to H^0, this benchmark is defined with a nonalignment ($c_{\beta-\alpha} \neq 0$) permitted by the constraints. In this case, the masses of A^0 and $H^\pm$ could be taken as degenerate, and the oblique parameters furthermore endorse that. Thus, they allow to decouple $m_{h^0} = 125 < m_{H^0} < m_{A^0} = m_{H^\pm}$, and the quartic couplings are set as $Z_4 = Z_5 = -2$. All the parameters are given in Table 2 (rows 1 and 2), and note that t_β and m_{H^0} are taken as free parameters.

- ***Scenario B***: In the previous scenario, it is assumed that the particle, which was discovered in 2012 at the LHC, is the h^0. However, that particle could also be the heavier CP-even Higgs (H^0) state. In that case, the coupling c_{H^0VV} will be scaled by a factor of $c_{\beta-\alpha}$ instead of $s_{\beta-\alpha}$, and that forces $s_{\beta-\alpha}$ to vanish. Besides, the couplings of h^0 to vector bosons (c_{h^0VV}) could not be large due to the limits set by the LHC. Therefore, it needs to be suppressed ($s_{\beta-\alpha} \to 0$). This scenario was presented in reference [23], and the conclusion was that the region of $65 < m_h < 120$ GeV was not rejected yet by the LHC particularly in the observations of $h^0 \to bb, \tau\tau$. As a result, an upper limit on t_β was presented. Furthermore, it was discussed that it is possible to set $c_{\beta-\alpha} = 0.9$ for Type I in the 2HDM [23]. Since there are no Higgs–fermion couplings in the scattering process, setting different Yukawa coupling schemes does not change the results. Therefore, the exact alignment and a small deviation from the alignment are considered in benchmark points 3 and 4. The parameters are given in the Hybrid base [23] in Table 2 (rows 3 and 4), where $Z_4 = Z_5 = -1$ is taken so that the oblique parameters cannot receive sizable contributions (Eq. (76) in reference [23]).

Table 2. Benchmark points for Scenario A (rows 1 and 2) and Scenario B (rows 3 and 4). All masses are given in GeV.

Benchmark points	m_{h^0}	m_{H^0}	$c_{\beta-\alpha}$	Z_4	Z_5	Z_7	t_β
bp-1	125	(150 . . . 600)	0.1	-2	-2	0	(2...50)
bp-2	125	(150 . . . 600)	0.01	-2	-2	0	(2...50)
bp-3	(65 . . . 120)	125	1.0	-1	-1	0	5
bp-4	(80 . . . 120)	125	0.9	-1	-1	0	5

It should be noted that the parameter regions given in Table 2 agree well with the vacuum stability, the perturbativity, and the perturbative unitarity constraints. The parameter regions are tested using 2HDMC-1.7.0 [41]. Since the couplings given in Table 1 are defined in Higgs mass basis, the conversion between the Hybrid basis to the Higgs mass basis is also accomplished with the help of 2HDMC. The relations between the

masses of $(m_{A^0}, m_{H^\pm})$ and the parameters of (Z_4, Z_5) are defined as follows:

$$m^2_{A^0} = m^2_{H^0} s^2_{\beta-\alpha} + m^2_{h^0} c^2_{\beta-\alpha} - Z_5 v^2, \quad (6)$$

$$m^2_{H^\pm} = m^2_{A^0} - 0.5(Z_4 - Z_5)v^2. \quad (7)$$

Setting $Z_4 = Z_5$ makes $m_{H^\pm} = m_{A^0}$, and note that parameter Z_5 takes part in the mass of the A^0 boson [23].

5. Numerical analysis and discussion

In this section, the results are presented for the following scattering processes: $\gamma\gamma \to H^+H^-h^0$ and $\gamma\gamma \to H^+H^-H^0$. The SM parameters are taken from reference [51], where $s_w = 0.22289$ and $\alpha(M_Z) = 1/127.944$ are set. The free parameters of the model are given for Scenarios A and B with two benchmark points in Table 2. Before presenting the results, we would like to underline that the cross-section for each of the processes is calculated for various polarization configurations too. These configurations are inspired by the ILC, where pol-1 (pol-2) is defined as a right-handed photon with +30% (+60%) polarization and a photon with -80% left-handed polarization [52, 53].

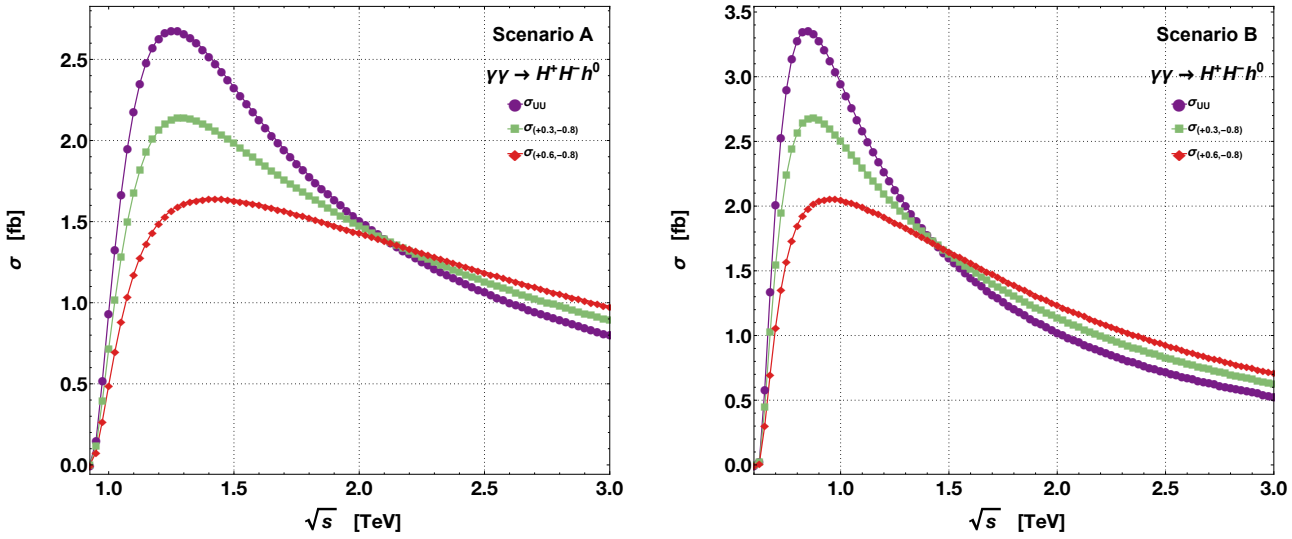

Figure 2. The integrated cross-section of $\gamma\gamma \to H^+H^-h^0$ as a function of $\hat{s}$. Left: Scenario A is given for $m_{h^0} = 125$ GeV, $m_{H^0} = 400$ GeV, $m_{H^\pm} \approx 530$ GeV, and $t_\beta = 10$. Right: Scenario B is given for $m_{h^0} = 90$ GeV, $m_{H^0} = 125$ GeV, $m_{H^\pm} \approx 265$ GeV, and $t_\beta = 5$.

In Figure 2, the cross-section distributions for $\gamma\gamma \to H^+H^-h^0$ are plotted. On the left (right), Scenario A (B) with two polarization cases of the incoming photons is given. It can be seen that the unpolarized cross-section σ_{UU} reaches up to 2.7 fb (3.4 fb) in Scenario A (B) around $\sqrt{\hat{s}} = 1.23$ TeV ($\sqrt{\hat{s}} = 1.6$ TeV), and then it falls. The cross-section for the polarized incoming photon beams is lower than the unpolarized one. They reach a maximum of $\sigma_{\text{pol-1}} \approx 2.2$ fb and $\sigma_{\text{pol-2}} \approx 1.55$ fb ($\sigma_{\text{pol-1}} \approx 2.7$ fb and $\sigma_{\text{pol-2}} \approx 2.05$ fb) for Scenario A (B). The polarized cross-sections are always less than the unpolarized ones in both of the processes because the helicity/polarization structure of the amplitude favors the opposite helicities, and indeed the contributions coming from σ_{LR} and σ_{RL} are significant. The other polarization states, σ_{LL} and σ_{RR}, are negligible. Since the unpolarized beam consists of 50% left-handed and 50% right-handed polarized photons, the scattering cross-

section is maximized for this configuration. The polarized incoming beam does not increase the cross-section necessarily compared to the electron–positron collisions with the s-channel diagrams.

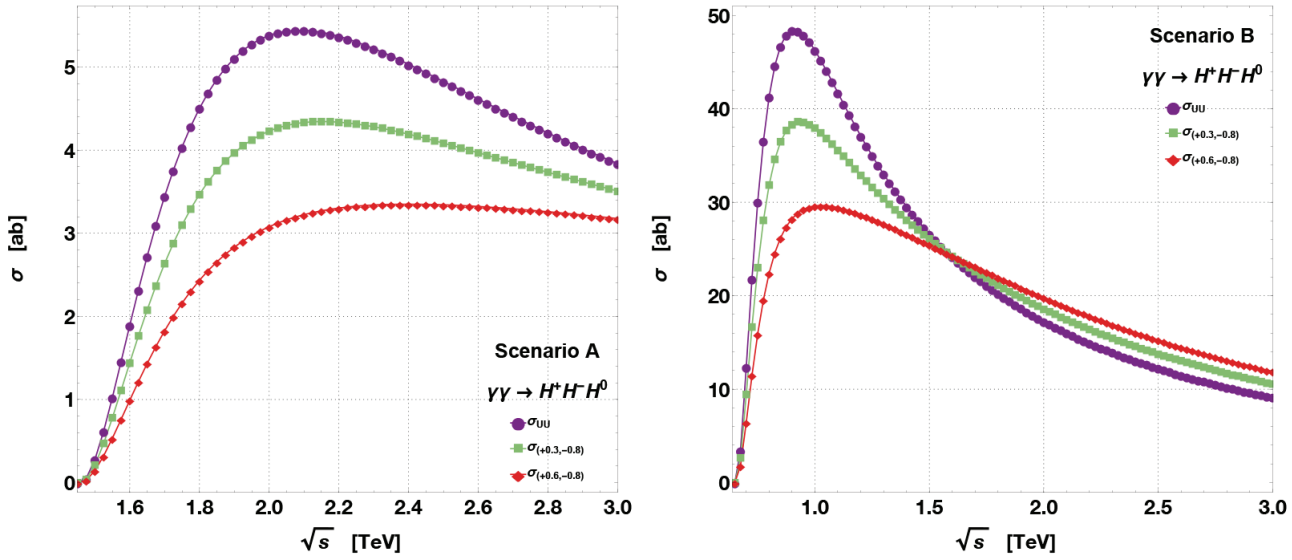

Figure 3. The integrated cross-section of $\gamma\gamma \to H^+H^-H^0$ as a function of $\hat{s}$. Left: Scenario A is assumed with $m_{h^0} = 125$ GeV, $m_{H^0} = 400$ GeV, $m_{H^\pm} \approx 530$ GeV, and $t_\beta = 40$. Right: Scenario B is given for $m_{h^0} = 90$ GeV, $m_{H^0} = 125$ GeV, $m_{H^\pm} \approx 265$ GeV, and $t_\beta = 5$.

Moving to the second process, the cross-sections of $\gamma\gamma \to H^+H^-H^0$ are given in Figure 3 for the same scenarios as a function of the c.m. energy. In Figure 3 (left), the unpolarized cross-section reaches up to 5.25 ab at $\sqrt{\hat{s}} \approx 2.15$ TeV for the benchmark point 1 in Scenario A. In Figure 3 (right), the cross-section rises moderately to $\sigma_{UU} = 49$ ab at $\sqrt{\hat{s}} \approx 0.8$ TeV for the benchmark point 4 in Scenario B. Obviously, the cross-section of this process is quite small, and it will be a challenge to explore this process in a $\gamma\gamma$-collider. The situation is the same for the pol-1 and pol-2 cases; both of them are smaller than the cross-section obtained with the unpolarized incoming beams.

The two-dimensional distributions of the cross-section as a function of m_{H^0} and t_β at $\sqrt{\hat{s}} = 2$ TeV for the scattering processes $\gamma\gamma \to H^+H^-h^0/H^0$ are given in Figure 4 (top row). The whole region defined in Scenario A is scanned by varying m_{H^0} and t_β. The figure on the left shows that the cross-section gets up to 30 fb at the top right corner where m_{H^0} and t_β are at the upper limits in the scenario. The increase in the cross-section is expected considering that coupling $|g_{H^+H^-h^0}|$ rises with the increasing values of m_{H^0} and t_β. On the other hand, the process $\gamma\gamma \to H^+H^-H^0$ still has a small cross-section, and it goes up to 9 ab around $m_{H^0} = 425$ GeV and high t_β values. Moreover, both of the trilinear Higgs self-couplings depend strongly on t_β, and so does their production cross-section. A similar analysis is obtained for Scenario B, where m_{h^0} changes with the limits defined in Table 2. In Figure 4 (bottom row, left), the process $\gamma\gamma \to H^+H^-h^0$ is plotted as a function of m_{h^0} where the cross-section for benchmark point 3 is higher for small values of m_{h^0}, and then it drops at a constant rate. The same discussion holds for the process $\gamma\gamma \to H^+H^-H^0$ given in Figure 4 (bottom row, right). Comparing these two processes shows that $\sigma(\gamma\gamma \to H^+H^-h^0)$ has quite a higher cross-section than $\sigma(\gamma\gamma \to H^+H^-H^0)$.

The last analysis is given for the total cross-section convoluted with the photon luminosity in an e^+e^--

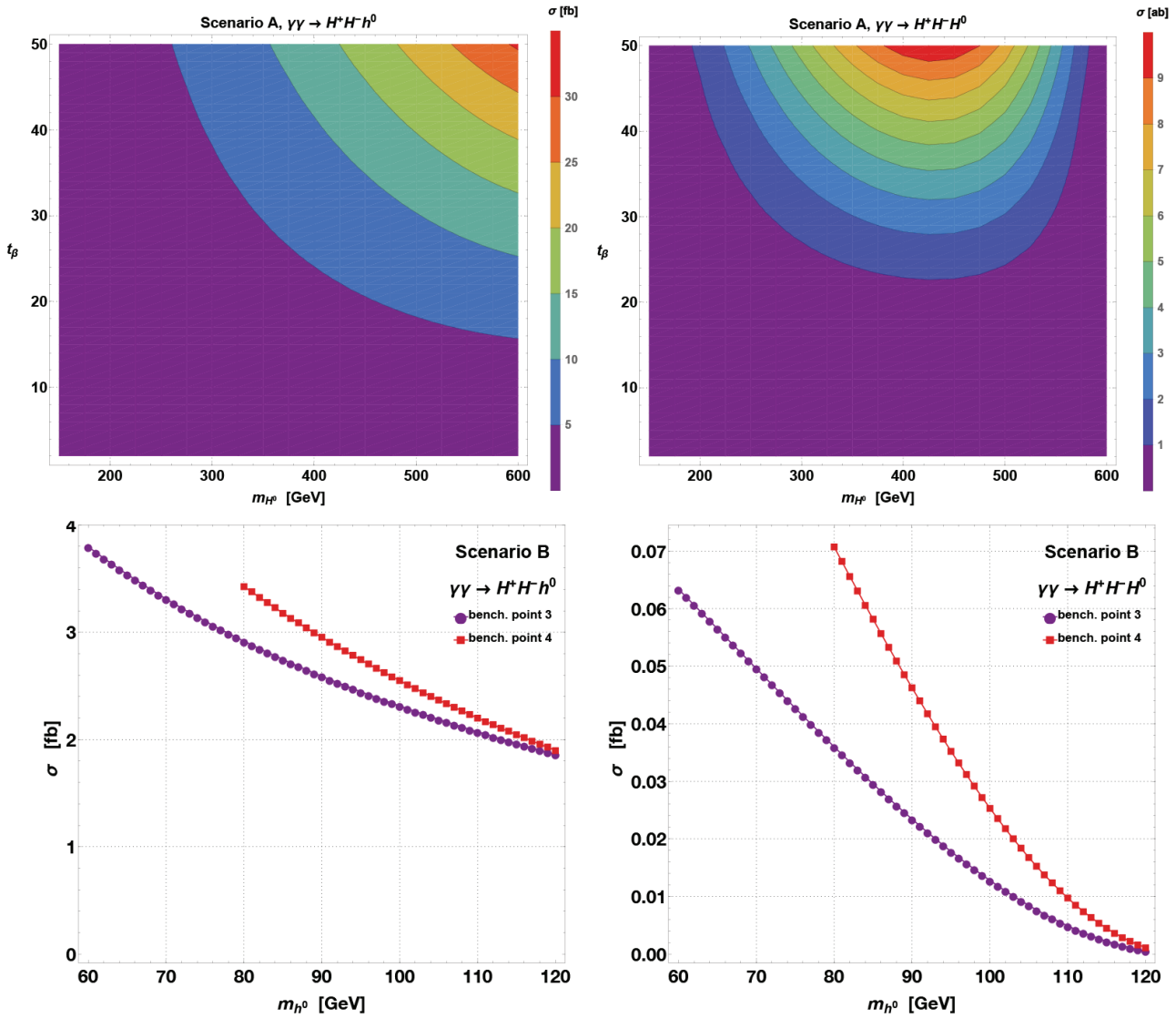

Figure 4. **Top row**: Scenario A is assumed with $m_{h^0} = 125$ GeV, $c_{\beta-\alpha} = 0.1$, and $Z_4 = Z_5 = -2$ as a function of m_{H^0} and t_β at $\sqrt{\hat{s}} = 2$ TeV. Left: The process $\gamma\gamma \to H^+H^-h^0$ is computed. Right: The process $\gamma\gamma \to H^+H^-H^0$ is assumed. **Bottom row**: Scenario B is given for $m_{H^0} = 125$ GeV, $c_{\beta-\alpha} = 1$, $Z_4 = Z_5 = -1$, and $t_\beta = 5$ as a function of m_{h^0} at $\sqrt{\hat{s}} = 1$ TeV. Left: The process $\gamma\gamma \to H^+H^-h^0$ is computed. Right: The process $\gamma\gamma \to H^+H^-H^0$ is assumed.

collider as a function of the c.m. energy, and the distributions are given in Figure 5. On the left, the process $e^+e^- \to \gamma\gamma \to H^+H^-h^0$ is plotted, and the total convoluted cross-section reaches up to 1.47 fb after $\sqrt{s} = 1.5$ TeV for bp-4. The bp-1 and bp-2 defined in Scenario A have a smaller total convoluted cross-section, and they are 0.99 fb and 1.15 fb, respectively. The bp-3 has a similar trend as bp-4, and it is just 13% lower than bp-4 for $\sqrt{s} > 1.4$ TeV. In Figure 5 (right), the same distributions for the process $e^+e^- \to \gamma\gamma \to H^+H^-H^0$ are plotted. The highest cross-section value is obtained with the same benchmark points in the previous process, and it is ≈ 22 ab around $\sqrt{s} = 1.8$ TeV in bp-4. The cross-section value is lower in the other benchmark points. Unfortunately, the total convoluted cross-section is too low to explore this process in a $\gamma\gamma$-collider, and it requires large total luminosity. The convoluted cross-section drops in all the processes at high c.m. energies

because the number of converted photons is decreased.

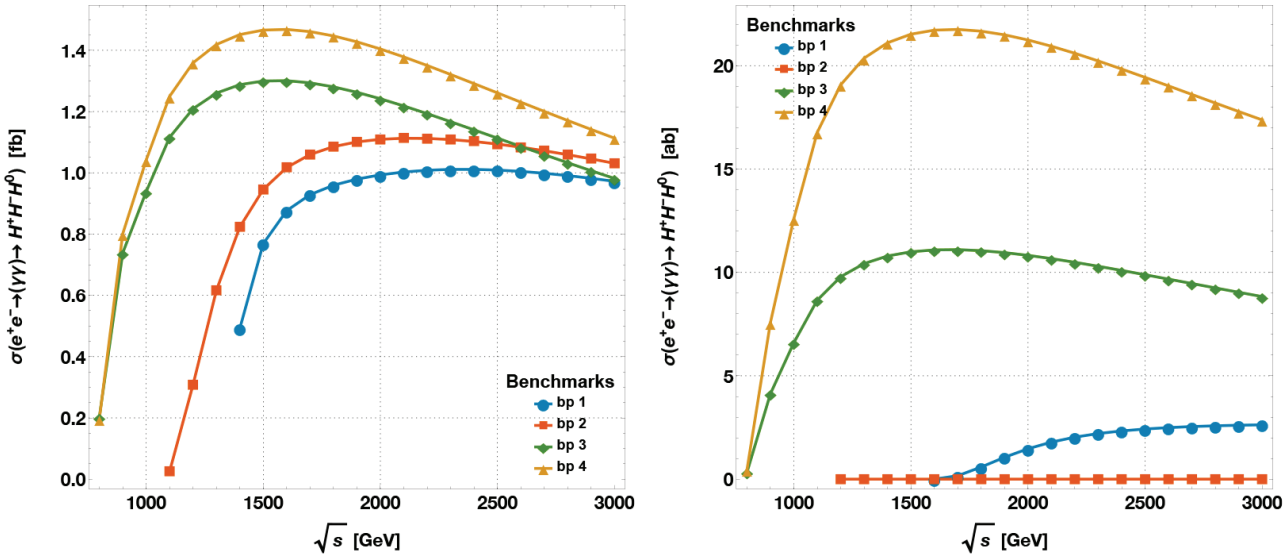

Figure 5. The total integrated cross-section with the photon luminosity in an e^+e^--collider as a function of c.m. energy. Left: The process $\gamma\gamma \to H^+H^-h^0$ with the same parameters given in the caption of Figure 2. Right: The process $\gamma\gamma \to H^+H^-H^0$ with the same parameters given in the caption of Figure 3.

6. Conclusion

In this study, the processes $\gamma\gamma \to H^+H^-h^0$ and $\gamma\gamma \to H^+H^-H^0$ are studied at tree-level in a $\gamma\gamma$-collider. The calculation is performed in the 2HDM, and the free parameters of the model are inspired by a recent study [23]. It should be underlined that these processes are not affected by the types of the Yukawa couplings, and that gives the opportunity to study the couplings of the charged Higgs pair to CP-even neutral Higgs bosons ($g_{H^+H^-[h^0,H^0]}$) without any interference from the other couplings in the 2HDM. Besides, the couplings $g_{H^+H^-h^0}$ and $g_{H^+H^-H^0}$ are the only triple Higgs self-couplings that include the charged Higgs bosons. Furthermore, these two scattering processes could be used for determining these couplings.

According to the results, Scenario B with benchmark point 4 has the highest production rate in both of the final states. The production rate of $H^+H^-h^0$ is high, and it could be possible to measure it. The production rate of $H^+H^-H^0$ is not so high because the cross-section is at the order of tens of attobarn, and the measurement of this process in a collider will be hard. The possible polarization cases of the incoming beams are studied as well in this paper; however, these polarization cases do not necessarily increase the cross-section, and, in fact, the unpolarized cross-section is better for having a higher number of events. The total convoluted cross-section in an e^+e^--collider with $\sqrt{s} > 2$ TeV is enough to gather the maximum number of events for benchmark point 4. A detailed simulation study is required for the full assessment of the collider, taking into account the acceptance and the decay chain of the neutral and the charged Higgs bosons. It should be stressed that these production channels do not compete in the search of the charged Higgs boson in e^+e^- and $\gamma\gamma$ colliders with the primary production channel (H^+H^-). This study presents the potential of a $\gamma\gamma$-collider in the context of charged Higgs boson searches and in determining the charged Higgs self-couplings in the 2HDM.

Acknowledgments

The computation reported in this study was partially performed at the TÜBİTAK ULAKBİM High Performance and Grid Computing Center (TRUBA resources) and the computing resource of FENCLUSTER (Faculty of Science, Ege University). Ege University supported this work with project number 17-FEN-054.

References

[1] Chatrchyan, S.; Khachatryan, V.; Sirunyan, A. M.; Tumasyan, A.; Adam, W.; Aguilo, E.; Bergauer, T.; Dragicevic, M.; Erö, J.; Fabjan, C. et al. *Phys. Lett. B* **2012**, *716*, 30-61.

[2] Aad, G.; Abajyan, T.; Abbott, B.; Abdallah, J.; Abdel Khalek, S.; Abdelalim, A. A.; Abdinov, O.; Aben, R.; Abi, B.; Abolins, M. et al. *Phys. Lett. B* **2012**, *716*, 1-29.

[3] Khachatryan, V.; Sirunyan, A. M.; Tumasyan, A.; Adam, W.; Bergauer, T.; Dragicevic, M.; Erö, J.; Fabjan, C.; Friedl, M.; Frühwirth, R. et al. *Eur. Phys. J. C* **2014**, *74*, 3076.

[4] Behnke, T.; Brau, J. E. ; Foster, B.; Fuster, J.; Harrison, M.; Paterson, J. M.; Peskin, M.; Stanitzki, M.; Walker, N.; Yamamoto, H. arXiv:physics.acc-ph/1306.6327.

[5] Linssen, L.; Miyamoto, A.; Stanitzki, M.; Weerts, H. *CERN Yellow Report CERN-2012-003*; arXiv:physics.ins-det/1202.5940, 2012.

[6] Yamamoto, A. In *PoS ICHEP2016*; 2017, 067.

[7] Gunion, J. F.; Haber, H. E.; Kane, G. L.; Dawson, S. *Front. Phys.* **2000**, *80*, 1-404.

[8] Martin, S. P. *Adv. Ser. Direct. High Energy Phys.* **2010**, *21*, 1-153.

[9] Coniavitis, E.; Ferrari, A. *Phys. Rev. D* **2007**, *75*, 015004.

[10] Asakawa, E.; Choi, S. Y.; Lee, J. S. *Phys. Rev. D* **2001**, *63*, 015012.

[11] Beccaria, M.; Ferrari, A.; Renard, F. M.; Verzegnassi, C. *DESY LC note: LC-TH-2005-005*, 2005.

[12] Hashemi, M. *Commun. Theor. Phys.* **2014**, *61*, 69-74.

[13] Sonmez, N. *Ege University Journal of the Faculty of Science* **2016**, *40*, 23-36.

[14] Ferrera, G.; Guasch, J.; López-Val, D.; Sola, J. *Phys. Lett. B* **2008**, *659*, 297-307.

[15] Hashemi, M.; Ahmed, I. *Int. J. Mod. Phys. A* **2015**, *30*, 1550022.

[16] Arhrib, A.; Benbrik, R.; Chen, C. H.; Santos, R. *Phys. Rev. D* **2009**, *80*, 015010.

[17] Ahmed, I. *Adv. High Energy Phys.* **2017**, 6139250.

[18] Shen, J. F.; Bi, Y. P. *Europhys. Lett.* **2014**, *105*, 41001.

[19] Hall, L. J.; Wise, M. B. *Nucl. Phys. B* **1981**, *187*, 397-408.

[20] Deshpande, N. G.; Ma, E. *Phys. Rev. D* **1978**, *18*, 2574-2576.

[21] Lavoura, L. *Phys. Rev. D* **1994**, *50*, 7089-7092.

[22] Branco, G. C.; Ferreira, P. M.; Lavoura, L.; Rebelo, M. N.; Sher, M.; Silva, J. P. *Phys. Rept.* **2012**, *516*, 1-102.

[23] Haber, H. E.; Stål, O. *Eur. Phys. J. C* **2015**, *75*, 491.

[24] Hahn, T. *Comput. Phys. Commun.* **2001**, *140*, 418-431.

[25] Hahn, T.; Rauch, M. *Nucl. Phys. Proc. Suppl.* **2006**, *157*, 236-240.

[26] Telnov, V. I. *Nucl. Instrum. Meth. A* **1990**, *294*, 72-92.

[27] Telnov, V. I. *Nucl. Instrum. Meth. A* **1995**, *355*, 3-18.

[28] Heuer, R.; Miller, D. J.; Richard, F.; Zerwas, P. M.; Aguilar-Saavedra, J. A.; Alcaraz, J.; Ali, A.; Ambrosanio, S.; Andreazza, A.; Andruszkow, J. et al. *DESY*, 2001, arXiv:hep-ph/0106315.

[29] Ginzburg, I. F.; Kotkin, G. L.; Panfil, S. L.; Serbo, V. G.; Telnov, V. I. *Nucl. Instrum. Meth. A* **1984**, *219*, 5-24.

[30] El Kaffas, A. W.; Khater, W.; Ogreid, O. M.; Osland, P. *Nucl. Phys. B* **2007**, *775*, 45-77.

[31] Sher, M. *Physics Reports* **1989**, *179*, 273-418.

[32] Nie, S.; Sher, M. *Phys. Lett. B* **1999**, *449*, 89-92.

[33] Ginzburg, I.; Ivanov, I. *Phys. Rev. D* **2005**, *72*, 115010.

[34] ALEPH Collaboration; DELPHI Collaboration; L3 Collaboration; OPAL Collaboration; SLD Collaboration; LEP Electroweak Working Group; SLD Electroweak Heavy Flavour Groups. CERN, 2005, arXiv:hep-ex/0509008.

[35] Peskin, M. E.; Takeuchi, T. *Phys. Rev. Lett.* **1990**, *65*, 964-967.

[36] Peskin, M. E.; Takeuchi, T. *Phys. Rev. D* **1992**, *46*, 381-409.

[37] Haber, H. E.; O'Neil, D. *Phys. Rev. D* **2011**, *83*, 055017.

[38] Gunion, J. F.; Haber, H. E. *Phys. Rev. D* **2003**, *67*, 075019.

[39] Grimus, W.; Lavoura, L.; Ogreid, O. M.; Osland, P. *Nucl. Phys. B* **2008**, *801*, 81-96.

[40] Polonsky, N.; Su, S. *Phys. Lett. B* **2001**, *508*, 103-108.

[41] Eriksson, D.; Rathsman, J.; Stal, O. *Comput. Phys. Commun.* **2010**, *181*, 189-205.

[42] Chatrchyan, S.; Khachatryan, V.; Sirunyan, A. M.; Tumasyan, A.; Adam, W.; Aguilo, E.; Bergauer, T.; Dragicevic, M.; Erö, J.; Fabjan, C. et al. *Phys. Lett. B* **2012**, *716*, 30-61.

[43] ALEPH Collaboration; DELPHI Collaboration; L3 Collaboration; OPAL Collaboration; LEP Working Group for Higgs Boson Searches. *Eur. Phys. J. C* **2013**, *73*, 2463.

[44] Abazov, V. M.; Abbott, B.; Abolins, M.; Acharya, B. S.; Adams, M.; Adams, T.; Aguilo, E.; Ahsan, M.; Alexeev, G. D.; Alkhazov, G. et al. *Phys. Rev. Lett.* **2009**, *102*, 191802.

[45] Abazov, V. M.; Abbott, B.; Abolins, M.; Acharya, B. S.; Adams, M.; Adams, T.; Aguilo, E.; Ahsan, M.; Alexeev, G. D.; Alkhazov, G. et al. *Phys. Rev. D* **2009**, *80*, 071102.

[46] Abazov, V. M.; Abbott, B.; Abolins, M.; Acharya, B. S.; Adams, M.; Adams, T.; Aguilo, E.; Ahsan, M.; Alexeev, G. D.; Alkhazov, G. et al. *Phys. Rev. D* **2009**, *80*, 051107.

[47] Aaltonen, T.; Adelman, J.; Akimoto, T.; Álvarez González, B.; Amerio, S.; Amidei, D.; Anastassov, A.; Annovi, A.; Antos, J.; Apollinari, G. et al. *Phys. Rev. Lett.* **2009**, *103*, 101803.

[48] Aad, G.; Abbott, B.; Abdallah, J.; Abdel Khalek, S.; Abdelalim, A. A.; Abdinov, O.; Abi, B.; Abolins, M.; AbouZeid, O. S.; Abramowicz, H. et al. *J. High Energy Phys.* **2012**, *6*, 39.

[49] Chatrchyan, S.; Khachatryan, V.; Sirunyan, A. M.; Tumasyan, A.; Adam, W.; Aguilo, E.; Bergauer, T.; Dragicevic, M.; Erö, J.; Fabjan, C. et al. *J. High Energy Phys.* **2012**, *7*, 143.

[50] Moretti, S. In *Proceedings of the Workshop on Prospects for Charged Higgs Discovery at Colliders (CHARGED2016); 3-6 October 2016; Uppsala, Sweden*.

[51] Eidelman, S.; Hayes, K.; Olive, K.; Aguilar-Benitez, M.; Amsler, C.; Asner, D.; Babu, K.; Barnett, R.; Beringer, J.; Burchat, P. et al. *Phys. Lett. B* **2004**, *592*, 1-5.

[52] Fujii, K.; Grojean, C.; Peskin, M. E.; Barklow, T.; Gao, Y.; Kanemura, S.; Kim, H.; List, J.; Nojiri, M.; Perelstein, M. et al. *arXiv e-prints:hep-ex/1506.05992*.

[53] CLIC and CLICdp Collaborations; Boland, M. J.; Felzmann, U.; Giansiracusa, P. J.; Lucas, T. G.; Rassool, R. P.; Balazs, C.; Charles, K.; Afanaciev, T. K.; Emeliantchik, I. et al. *arXiv e-prints:physics.acc-ph/1608.07537*.